Dalton Transactions

ROYAL SOCIETY OF CHEMISTRY

PAPER

View Article Online
View Journal | View Issue

Cite this: *Dalton Trans.*, 2025, **54**, 9388

Reactivity of trinuclear ruthenium acetates with nitrite and nitric oxide ligands in aqueous media†

Hugo E. Barbosa, [a] Amanda B. da Silva, [a] Pedro H. O. Nazar, [a] Renan R. Bertoloni, [a] Antonio G. S. de Oliveira-Filho[a,b] and Sofia Nikolaou *[a]

The chemical reactivity of nitrosyl- and nitrite-coordinated compounds in an aqueous environment is a vital part of understanding the action of these compounds as potential nitric oxide-releasing molecules (NORMs). This work reports the behaviour of the $[Ru_3O(CH_3COO)_6(py)_2NO_2]$ (**1**) complex, which is an isomeric mixture of nitrite-N and nitrite-O, and the nitrosyl complex $[Ru_3O(CH_3COO)_6(py)_2NO]PF_6$ (**2**) in aqueous medium with and without light irradiation. NO release under light irradiation was detected through chronoamperometry, which showed that nitrite complex **1** produces NO but is less effective than nitrosyl complex **2**. This difference is due to the mechanism of NO production by complex **1**, which depends on the nitrite-O isomer, present in minor proportion in the synthetic sample, as shown by computational and NMR data. The reactivity of these compounds in the dark was investigated under various pH values. The nitrite complex **1** had the coordinated nitrite converted to NO^+, with a pK = 4.2. NO^+ was readily released, yielding the solvate species $[Ru_3O(CH_3COO)_6(py)_2S]^+$. For the nitrosyl complex **2**, two successive nucleophilic attacks by hydroxide ions were observed producing the $[Ru_3O(CH_3COO)_6(py)_2HNO_2]$ (**3**) and $[Ru_3O(CH_3COO)_6(py)_2NO_2]^-$ (**4**) compounds, with pK values of 9.8 and 12.3, respectively. In buffered solutions (TRIS.HCl and PBS), the kinetic trace for the conversion of **2** to **3** suggested an induction period followed by the complete conversion to $[Ru_3O(CH_3COO)_6(py)_2HNO_2]$ at pH values where the nitrosyl $[Ru_3O(CH_3COO)_6(py)_2NO]^+$ should be the major species. Based on these observations, our data suggest a sequence of steps in which compound **3** accumulates and then, with the aid of the buffer components, increases the rate of its own formation.

Received 15th March 2025,
Accepted 9th May 2025

DOI: 10.1039/d5dt00630a

rsc.li/dalton

Introduction

Reactive oxygen species (ROS) are defined as small and highly reactive oxygen-derived molecules such as hydrogen peroxide (H_2O_2), hydroxyl radical ($^{\bullet}OH$), singlet oxygen ($^1O_2$) and peroxyl radicals ($ROO^{\bullet}$).[1–3] Although these molecules are widely known for causing oxidative stress and DNA damage in controlled conditions, ROS act as cellular messengers regulating key physiological processes.[1,2,4–7] Similarly, the literature defines the so-called reactive nitrogen species, RNS, among which nitric oxide (NO) has received significant attention in the last 45 years. This is due to its role in several biological processes, such as vasodilation, reproduction, insulin secretion and neurotransmission.[8,9] Besides that, NO has also shown prominent activity as an anticancer, antibacterial, anti-inflammatory and vasodilator agent.[8–11]

Researchers seek to develop NO-releasing molecules (NORMs) composed of organic and inorganic moieties that can supply nitric oxide in specific sites for disease treatments.[9,12,13] The NO release by these compounds can result from the redox process, light irradiation, reaction with biomolecules and change in the pH environment.[8,9] Considering these factors and that nitric oxide affinity for transition metals is highly dependent on the electronic configuration of the metal, the use of nitrosyl coordination compounds as NORMs is desirable since the NO delivery can be easily triggered by redox process on the metal core or by photochemical process.[14,15]

In recent years, our research group has been studying the μ-oxo trinuclear ruthenium clusters as potential NORMs, showing that the complexes with the formula $[Ru_3O(CH_3COO)_6(L)_2NO]PF_6$ (L being a pyridinic ligand) have activity against cancer cells and can provide vasodilatation action,

[a]*Departamento de Química, LABiQSC[2] – Laboratório de Atividade Biológica e Química Supramolecular de Compostos de Coordenação, Faculdade de Filosofia, Ciências e Letras de Ribeirão Preto, Universidade de São Paulo, ZIPCODE 14040-901, Ribeirão Preto-SP, Brazil. E-mail: sofia@ffclrp.usp.br*

[b]*Instituto de Química de São Carlos, Universidade de São Paulo, Av. Trabalhador São-Carlense, 400, 13566-590 São Carlos-SP, Brazil*

†Electronic supplementary information (ESI) available: ^1H NMR, molecular modeling data, electronic absorption spectra for comparison of the compounds produced in the pK determination experiments, data from the Griess experiments, information of syntheses and kinetics curves under other conditions. See DOI: https://doi.org/10.1039/d5dt00630a

being these results related to light irradiation and reactions with biological reductants.[13,16] Despite these promising results, the reactivity of these nitrosyl complexes in aqueous environments due to pH influence and redox processes is unknown, making understanding the biological activities challenging.

In addition, the interest in the reactivity of the nitrite analogues relies on the fact that nitrite species are the most common product generated in aqueous media, depending on the pH, due to reactions at Ru–NO sites.[17,18] The conversion Ru–NO to Ru–NO_2^- is assigned to a nucleophilic attack by hydroxyl ions, and it is well established in the literature for mononuclear ruthenium compounds with higher NO^+ character.[19,20] However, this equilibrium was never reported for the triruthenium clusters, where the Ru–NO bond has a multiconfigurational character, being represented as $[\{Ru–NO\}^6Ru^{III}Ru^{III}O(CH_3COO)_6(py)_2]PF_6$, following the Enemark-Feltham notation.[21,22] A recent computational study from our group described this multiconfigurational character, showing the predominance of the Ru^{III}–NO^0 configuration.[22]

This work aimed to unveil the aqueous reactivity of such ruthenium nitrosyls, using compounds $[Ru_3O(CH_3COO)_6(py)_2NO_2]$ (**1**) and $[Ru_3O(CH_3COO)_6(py)_2NO]PF_6$ (**2**) as models (Fig. 1), leading, ultimately, to the examination of the paths involved in NO release, with and without light irradiation.

Experimental section

Materials

Hydrochloric and citric acid were purchased from Synth. Sulfuric and phosphoric acid were purchased from Êxodo. Sodium hydroxide pellets were purchased from Dinâmica. Acetonitrile, dichloromethane, dimethylformamide, dimethyl sulfoxide, hydrazine monohydrate, *N*-(1-naphthyl)-ethylenediamine dihydrochloride, ruthenium(III) chloride, sodium nitrite, sulfanilamide, phosphate buffered saline (PBS) pellets, neutral aluminium oxide, dibasic sodium phosphate and tris(hydroxymethyl)aminomethane were purchased from Sigma-Aldrich. The PBS pellets yield a 0.01 M phosphate buffer, 0.0027 M KCl and 0.137 M NaCl in 200 mL of deionized water. TRIS.HCl buffer was prepared by dissolving tris(hydroxymethyl)aminomethane in deionized water, adjusting the pH with HCl or NaOH solutions (0.1 M). All reagents and solvents were used as received.

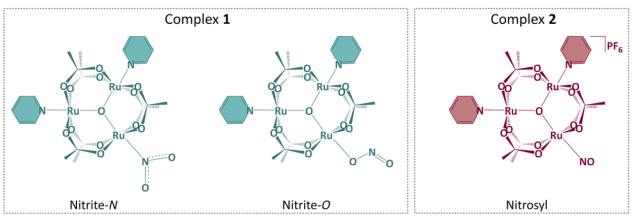

Fig. 1 Structure of the complexes studied in this work. Complex **1** was represented by two structures due to the presence of linkage isomers.

Synthesis of ruthenium complexes. The precursor $[Ru_3O(CH_3COO)_6(py)_2CH_3OH]PF_6$, and the compounds $[Ru_3O(CH_3COO)_6(py)_2NO_2]$ and $[Ru_3O(CH_3COO)_6(py)_2NO]PF_6$ were obtained according to adaptations of previously reported procedures.[21,23–25]

$[Ru_3O(CH_3COO)_6(py)_2NO_2]\cdot H_2O$ (1). 250 mg (0.247 mmol) of $[Ru_3O(CH_3COO)_6(py)_2(CH_3OH)]PF_6$ was dissolved in 20.0 mL of purified dimethylformamide. Then 99.8 mg (1.45 mmol) of $NaNO_2$ was added to the solution, stirring overnight at room temperature. The next day, the solvent was removed under reduced pressure, and the solid residue was then subjected to adsorption column chromatography with a neutral aluminium oxide (Al_2O_3) stationary phase. When the mobile phase was dichloromethane/acetonitrile 1 : 4, the first brown fraction was obtained, identified as $[Ru_3O(CH_3COO)_6(py)_2(NO)]PF_6$. The second fraction was collected using the mobile phase methanol/acetonitrile/dichloromethane (1 : 14 : 35). This fraction was evaporated to dryness, and the resulting solid was dried under vacuum, yielding 117 mg of the product $[Ru_3O(CH_3COO)_6(py)_2(NO_2)]\cdot H_2O$ (MM = 895.69 g mol^{-1}; 0.131 mmol; η = 52%). UV-Vis (dichloromethane)/nm 322 (9032 M^{-1} cm^{-1}), 686 (5050 M^{-1} cm^{-1}); ^{1}H-NMR (400 MHz, ($CDCl_3$)), δ/ppm: nitrite-N 3.29 (d), 6.61 (t), 7.30 (t), 2.87 (s), 7.94 (s). Nitrite-O −0.23 (d), 5.62 (t), 6.19 (t), 3.88 (s), 3.01 (s). FT-IR (KBr)/cm^{-1}: 821 and 837 (δ ONO), 1295 (ν_s (NO_2)), 1323 (ν_{as} (NO_2)), 1367 (ν (ON═O)), 1423 (ν_s (COO)Ac), 1589 (ν_{as} (COO)Ac). Elemental analysis, calcd for $C_{22}H_{30}N_3O_{16}Ru_3$ (%) C = 29.50%; H = 3.38%; N = 4.69%; experimental (%) C = 29.20%; H = 3.39%; N = 4.65%.

$[Ru_3O(CH_3COO)_6(py)_2NO]PF_6$ (2). 541 mg of $[Ru_3O(CH_3COO)_6(py)_2(CH_3OH)]PF_6$ was dissolved in 52.5 mL of dichloromethane. This solution was kept under argon flow for 1 hour. The solution was then kept under a flow of gaseous nitric oxide generated from the reaction between a 1.00 M H_2SO_4 solution and an aqueous $NaNO_2$ solution. The NO saturation was maintained for 3 hours, and the reaction mixture was evaporated to dryness. The solid was purified using adsorption column chromatography with a neutral alumina (Al_2O_3) stationary phase with a 1 : 1 dichloromethane/acetonitrile mobile phase. This fraction was evaporated to dryness, and the resulting solid was dried under vacuum, yielding 79.1 mg of the product. $[Ru_3O(CH_3COO)_6(py)_2(NO)]PF_6$ (MM = 1006.64 g mol^{-1}; 0.0785 mmol; η = 46%). UV-Vis (acetonitrile)/nm 451 (3130 M^{-1} cm^{-1}), 538 (2840 M^{-1} cm^{-1}), 691 (1740 M^{-1} cm^{-1}); ^{1}H-NMR (400 MHz, (CD_3CN)), δ/ppm: 8.10 (s, 4H), 5.83 (s, 2H,), 4.52 (s, 4H) 3.96 (s, 6H), 3.29 (s, 12H). FT-IR (KBr)/cm^{-1}: 841 (ν PF_6), 1431 (ν_s (COO)Ac), 1592 (ν_s (COO)Ac), 1901 (νNO). Elemental analysis, calcd for $C_{22}H_{28}N_3O_{14}Ru_3PF_6$ (%) C = 26.25%; H = 2.80%; N = 4.17%; experimental (%) C = 25.85%; H = 2.87%; N = 4.17%.

Physical measurements

The UV-Vis electronic spectra were recorded using an Agilent Cary-60 spectrophotometer with a spectral range of 190 to 1100 nm and a quartz cuvette with a 1.0 cm path length. The infrared spectra of the complexes were collected on a Shimadzu IR Prestige 21 spectrophotometer, from 400 to

4000 cm^{-1}, with a resolution of 4 cm^{-1}. The release of NO was detected using a selective electrode (NOmeter, Noximeter Insight) inside the cuvette, and irradiation was performed with a laser tag Colibri Quantum Laser Tech.

Monitoring of nitric oxide release using a selective electrode

The photolysis of the complexes $[Ru_3O(CH_3COO)_6(py)_2NO]PF_6$ and $[Ru_3O(CH_3COO)_6(py)_2NO_2]$ were performed in aqueous solution. Since the complexes are partially soluble in water, a stock solution of the complexes in dimethylsulfoxide (2.25 mM) was prepared, and a 60.0 μL aliquot of this stock solution was added to 3.00 mL of water in a quartz cuvette, resulting 45.0 μM concentration. The solutions were continuously stirred during irradiation, which was performed at λ_{irrad} = 377 nm.

Determination of the $NO^+(NO^0)/NO_2^-$ conversion equilibrium constant

For complex **1**, pH 0–2 solutions were prepared using dilute HCl and 0.100 M citrate/citric acid buffer solutions with a pH range of 2.5–6.5. In the case of the buffered solutions, pH corrections were made using minimum volumes of HCl and NaOH solutions. For each measurement, 4.00 mL of the corresponding pH solution and 200 μL of a 1.97 mM solution of the complex in methanol were mixed, and spectral monitoring was carried out in the ultraviolet-visible region for 5 days at 35 °C. For complex **2**, pH 1 to 14 solutions were prepared by adding sodium hydroxide or hydrochloric acid and measuring the pH using a previously calibrated pH meter. For each measurement, 3.00 mL of the corresponding pH solution and 650 μL of a 0.60 mM solution of **2** in acetonitrile were mixed, and spectral monitoring was carried out in the ultraviolet-visible region for 30 min at 35 °C. The initial concentration of the complex was 0.10 mM in each measurement, and all the experiments were carried out under light protection. The p*K* values were determined in both cases from the first derivative of a sigmoid plot of absorbance *vs.* pH.

GRIESS reagent test

The reagent solution was made by adding 5.00 mL of 85% phosphoric acid to 30.0 mL of deionized water. 500 mg of sulfanilamide and 50.0 mg of *N*-(1-naphthyl)-ethylenediamine dihydrochloride were added to this solution. The volume was topped up to 50.0 mL, and the solution was stored in a volumetric flask in the refrigerator, which has been stable for about a month. In the experiment, 1.00 mL of the reagent solution was mixed with 1.00 mL of complex **1** solution at a concentration of 45.0 μM in water using 2% DMSO as a co-solvent. The analytical curve was made using $NaNO_2$ in the concentration range from 20.0 to 75.0 μM.

Reactivity of the nitrosyl complex 2 in aqueous media using buffer solutions

Aqueous solutions of TRIS.HCl buffer (0.01 M, pH 7.4 and 8.5) and PBS (0.01 M, pH 7.4) were prepared, adjusting their pH with additions of NaOH and HCl and checking on a pH meter. To 3.00 mL of each of these solutions, it was added 60.0 μL of a solution in acetonitrile of the complex $[Ru_3O(CH_3COO)_6(py)_2NO]PF_6$, resulting in a concentration of 0.100 mM. The solutions were kept protected from light, and the reactivity of the complex was monitored over time at room temperature using electronic absorption spectra. Kinetic curves were recorded at 470 nm (consumption of **2**) in the electronic absorption spectrum. The rate constant (k_{obs}) was determined by a single exponential fit after the induction period (1680 s for TRIS.HCl at pH 7.4 and 1560 s for PBS pH 7.4).

Reactivity of the nitrosyl compound 2 at different pHs in the absence and presence of salts

Compound **2** (0.100 mM) was subjected to two aqueous solutions of pH 5 and pH 10 (prepared by adding aliquots of 0.100 M HCl or NaOH solutions). At pH 10, the formation of **3** was monitored and a kinetic curve was generated at 556 nm (λ_{max} of **3**), obtaining a kinetic constant (k_{obs}) from a simple exponential fit. Still at pH 10, **2** (0.100 mM) and 100 μL of a stock solution containing tris(hydroxymethyl)aminomethane in 500-fold excess of the complex were added. The solution pH 10 were adjusted with small amounts of 1.00 M NaOH and HCl. In addition, electronic spectra were recorded at different times at room temperature and in the dark. The same was done using tris(hydroxymethyl)aminomethane at pH 5 and dibasic sodium phosphate at pH 10.

Molecular modeling

Density functional theory (DFT) calculations, using the ORCA program,[26] were performed to investigate the relative stability of the isomers of compound **1**. Geometry optimizations, vibrational harmonic frequencies, and thermochemical calculations for all structures were performed using the B97 density functional[27] and the def2-TZVP basis set.[28] All structures studied in this work were optimized in dimethylformamide solution using the CPCM solvation model.[29] The nature of the optimized structures was confirmed as minima by the harmonic vibrational frequency calculations with no imaginary frequencies.

Results and discussion

Photochemical production of nitric oxide

The primary interest in studying metallic nitrosyls is their potential application as controlled NO-releasers. The photoinduced delivery of NO from ruthenium-nitrosyls is known in the literature.[30] Our group has previously associated the photochemical release of nitric oxide from nitrosyl triruthenium clusters with their anticancer and vasodilatation properties.[13,30,31] Upon irradiation at the cluster-to-ligand charge-transfer transitions (CLCT), NO release occurs due to the population of the π-antibonding orbitals of NO and the weakening of π-backbonding. Irradiation at 660 nm, in the intra-cluster transition (IC), does prompt NO release, but with much less efficiency, in such a way that NO is not detected by

absorption electronic spectroscopy and amperometric monitoring. Nevertheless, we measured its release using indirect luminescence measurements and verified that the efficacy of vasodilation increases under ambient light exposure.[31] On the other hand, coordinated NO undergoes nucleophilic attack in aqueous media, mainly by OH^- ions, in a pH-dependent manner.[19,32,33] Consequently, for some ruthenium-nitrosyls, the actual species at physiological pH might be the corresponding nitrite complex, which has led to interest in studying the ability of these nitrites to release NO. Precedents of NO release by photoinduction from nitrite ruthenium complexes have been described,[34–36] driving our attention to compound **1** as a potential photoNORM.

As shown in Fig. 2, under the same experimental conditions, irradiation of **1** and **2** at 377 nm leads to the NO release and, as expected, with higher efficiency from **2**, the nitrosyl compound. Chronoamperometry showed immediate NO detection after light triggering at 100 seconds for **2**, and an induction time of about 50 seconds for appreciable amounts of NO to be detected from **1**. A plato of current, signaling equilibrium in NO production, is also reached at different times, being faster for compound **2**. The difference in current detected between the complexes indicates that the amount of nitric oxide released from complex **1** is significantly lower than that of **2**.

There are examples in the literature showing NO production in aqueous medium by irradiation of mononuclear ruthenium compounds, where the nitrite-O isomer was identified as the main NO releaser. The mechanism involves the cleavage of the bond between the coordinated oxygen atom and the NO group of the NO_2^-, yielding free nitric oxide and a hydroxo compound, which can be further hydrolyzed to give the aqua compound, the final product of irradiation.[34] Cluster **1** consists of a mixture of linkage isomers, *i.e.*, $\{Ru^{III}NO_2\text{-}\kappa N\}$ referred to here as the ruthenium nitrite-N complex and $\{Ru^{III}NO_2\text{-}\kappa O\}$ as the ruthenium nitrite-O complex. Ohtsu and co-workers verified the occurrence of this isomeric mixture,[25] and we confirmed it by NMR (Fig. S1†). However, the assignment of which isomer occurs in higher quantity was not straightforward. The ^1H NMR spectrum of the compound isolated by us displayed two groups of signals, with a relative intensity ratio of about 6.5 : 1. The identification of the most abundant isomer in the sample was made based on the inductive and diamagnetic anisotropic effects of the N-bound linkage isomer (Fig. S2†). The nitrogen atom shields more effectively neighbour nuclei than oxygen. Besides that, the electron circulation in the N═O double bond creates an induced magnetic field that adds to the applied one, reinforcing the shielding effect and resulting, in the end, in higher values for the chemical shifts of the hydrogens of the nitrite-N isomer.

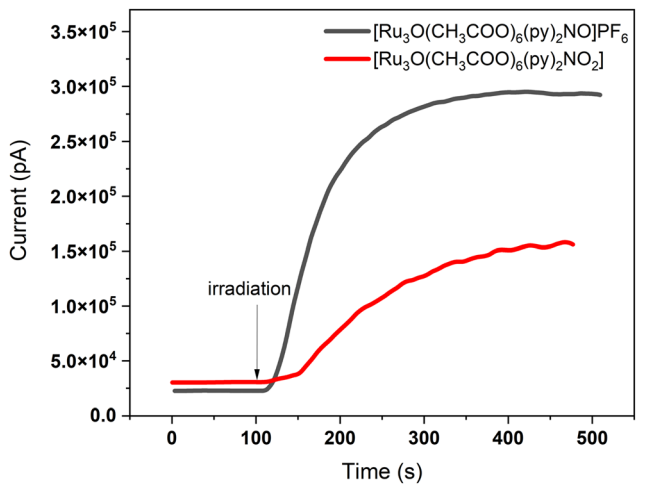

Fig. 2 Chronoamperogram of NO release from complexes **1** and **2** at 44.5 μM in water with 2% DMSO with irradiation after 100 s (λ_{irr} = 377 nm) at 298 K.

Molecular modeling calculations corroborated that result by considering the equilibrium between the N- and the O-bounded species (Fig. S3†). The free energy change for the reaction of isomerization from the nitrite-N to the nitrite-O form is ΔG = 14.7 kJ mol^{-1}, from which the equilibrium constant was calculated, $K_{eq} = 2.64 \times 10^{-3}$. This result revealed that the formation of the nitrite-O isomer is thermodynamically unfavourable, with a low formation constant, indicating that the nitrite-N species is the most stable in the synthesis solvent and, therefore, will be the species present in more significant amounts.

Therefore, we propose that the nitrite-O isomer is responsible for NO release from compound **1**. The fact that it is present as the minority fraction responds to the lower efficiency in release NO as compared to compound **2**.

pH-Dependent reactivity of compound 1

Complexes containing NO_2^- ligands react in aqueous media with H^+ ions, generating species that have NO^+ coordinated, and this is usually a reversible equilibrium.[36,37] Here, it is important to note that compounds **1** ($[Ru_3O(CH_3COO)_6(py)_2NO_2]$) and **2** ($[Ru_3O(CH_3COO)_6(py)_2NO]PF_6$) have a different number of electrons in their $[Ru_3O]$ core. Complex **1** has 17 electrons in this metal unit, while complex **2** has 18. This electron count sums 5 electrons per Ru(III) ion and 2 from the oxide anion, yielding a formal $[Ru^{III}Ru^{III}Ru^{III}O]$ metallic unit. For complex **2**, an extra electron comes from the NO^0 ligand, yielding a $[\{Ru\text{–}NO\}^6Ru^{III}Ru^{III}O]$ unit. Therefore, about the acid–base reactivity, there is no direct correlation between compounds **1** and **2**, and there is no expectation to observe the pH-dependent conversion of **1** to **2**, but rather to verify the eventual formation of the $[\{Ru\text{–}NO\}^5Ru^{III}Ru^{III}O]$ species. The latter, in turn, corresponds to a formal Ru(III) ion coordinated to a NO^+ ligand, a more π-receptor species than NO^0. We expected that the bond in the $\{Ru\text{–}NO\}^5$ fragment would be weak since the metal centre does not have enough electronic density to be involved in the π-backbonding with NO^+.[38,39] Then, in solution, the NO^+ replacement by a solvent molecule such as H_2O would be favourable and possibly fast, resulting in the solvate compound $[Ru_3O(CH_3COO)_6(py)_2S]^+$. The comparison between the spectra of compounds **1**, **1** after

HCl addition and the precursor $[Ru_3O(CH_3COO)_6(py)_2CH_3OH]^+$ (Fig. S4†) pointed to this result. As compound **1** is a mixture of linkage isomers, in an acidic environment the conversion to the respective NO species could be affected by the presence of such isomers. In addition, the release of NO itself could be affected depending on the ligand atom coordinated to the Ru(III) ion in the cluster. However, we have considered two aspects: the most important of which is that what actually reduces the affinity of NO for the metal center is its electronic deficiency. In other words, the Ru(III)–NO^+ bond is not expected to persist after the coordinated nitrite is converted to NO^+. This electronic effect is greater than others, regardless of which ligand atom is directly coordinated to the metal center. The second aspect is that, in any case, monitoring these reactions using conventional UV-visible spectroscopy does not allow us to observe any equilibrium or species other than the release of NO into solution or the formation of the solvate species. We have attempted to monitor these reactions using infrared spectroscopy. However, unlike mononuclear compounds, the infrared spectrum of the clusters is dominated by the intense bands of the bridged acetate groups, making it impossible to accurately follow the vibrations of nitrite in particular.

The Griess test was performed to address the labilization of the NO^+ ligand adequately. The Griess reagent is a probe to NO^+ in solution. In this method, NO^+ reacts with sulfanilamide (SA) in an acidic medium to form a transient diazonium salt. Through this intermediate, another reaction takes place with the coupling reagent, *N*-naphthyl-ethylenediamine (NED), to form a stable azo compound with absorption at 540 nm (pink color, the sequence of reactions is described in Fig. S5†).[40,41] Fig. S6† shows the color changes seen during the experiment. Compound **1** is subjected to acid conditions since the testing solution has a pH between 2.0 and 2.5 (see the Experimental section). Therefore, due to the formation of the azo dye, which has an absorbance at 540 nm, it was possible to demonstrate that the change in the color of the Griess test solution is a consequence of the release of NO^+ generated by the reaction of the $[Ru_3O(CH_3COO)_6(py)_2NO_2]$ complex with H^+ ions (Fig. S7†).

Since the conversion of the nitrite complex **1** to the corresponding solvate compound was verified, a p*K* value was determined (Fig. 3). This p*K* = 4.2 is taken here as an apparent equilibrium constant since the pH-dependent conversion of **1** to the solvate compound $[Ru_3O(CH_3COO)_6(py)_2S]^+$ involves two consecutive reactions, the conversion to the nitrosyl $[\{Ru–NO\}^5Ru^{III}Ru^{III}O(CH_3COO)_6(py)_2]^{2+}$, followed by a rapid aquation. The intermediate was not observed under the conditions of our experiments. In conclusion, compound **1** is a NO^+ releaser under acidic conditions.

pH-Dependent reactivity of compound 2

In analogy to the reactivity observed for mononuclear ruthenium nitrosyls, it is expected that compound **2**, $[\{RuNO\}^6Ru^{III}Ru^{III}O(CH_3COO)_6(py)_2]^+$, undergoes a pH-dependent nucleophilic attack reaction, in which coordinated NO reacts with OH^-.[19,32,33] The tricky aspect of studying this reaction is the fact that the complex **1** investigated in this work, $[Ru^{III}Ru^{III}Ru^{III}O(CH_3COO)_6(py)_2NO_2]$, is not the expected product in this reaction, as it contains one less electron in its metallic unit, as discussed in the previous section. The species isoelectronic to nitrosyl **2**, and therefore, the product of the nucleophilic attack reaction by hydroxyl ions is the complex $[Ru^{III}Ru^{III}Ru^{II}O(CH_3COO)_6(py)_2NO_2]^-$ (**4**). For comparison purposes, an attempt was made to obtain this species. However, since it could not be isolated, it was obtained *in situ* by reducing complex **1** with a stoichiometric amount of hydrazine in DMSO. Compound **4** electronic spectrum shows the CLCT charge transfer band at 385 nm and the IC intra-cluster band at 889 nm, a typical profile observed for so-called reduced clusters (Fig. S8†).[30]

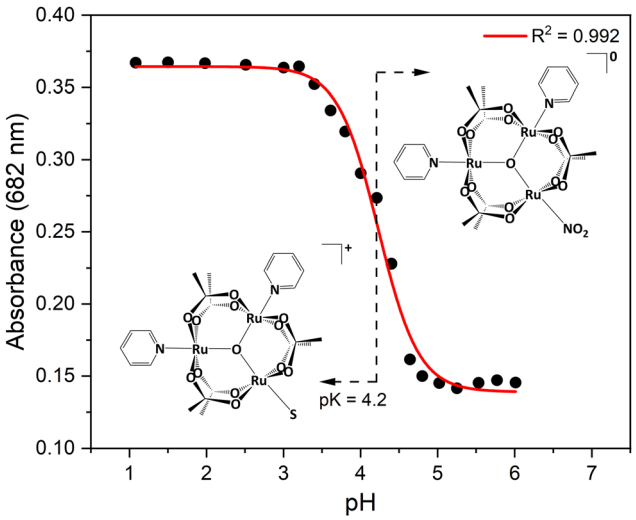

Fig. 3 Sigmoidal fit of the photometric monitoring data collected for complex **1** ($\lambda_{máx}$ = 682 nm) in aqueous solutions at different pH values.

Spectrophotometric monitoring of aqueous HCl and NaOH solutions at different pH values was then carried out on nitrosyl **2**. The complex remained intact in the pH 1–9 range, as seen by the persistence of the bands at 455 and 547 nm, and generated two other species between pH 10 and 13 (Fig. 4). At pH 13, the appearance of a band with an absorption maximum at λ_{max} = 882 nm indicates the formation of complex **4** (Fig. 4 and S8†). Between pH 10 and 13, the intermediate formed shows a spectral profile not yet reported in the literature. This species has been tentatively attributed to the compound $[Ru^{III}Ru^{III}Ru^{II}O(CH_3COO)_6(py)_2(HNO_2)]^0$ (compound **3**, λ_{max} = 561 nm in aqueous solution), and the proposed sequence of reactions is shown in Scheme 1. The literature considers the coordinated HNO_2 species to be the product of the first nucleophilic attack by hydroxyl ions on coordinated NO, although it is not usually observed.[36,37] The p*K* values for the successive equilibria were calculated from the first derivative of the sigmoid curve obtained from the graph of absorbance variation at 561 nm (compound **3**) and 882 nm (compound **4**) *versus* pH, Fig. 5. The relatively high pH values observed for these successive equilibria, especially for the first

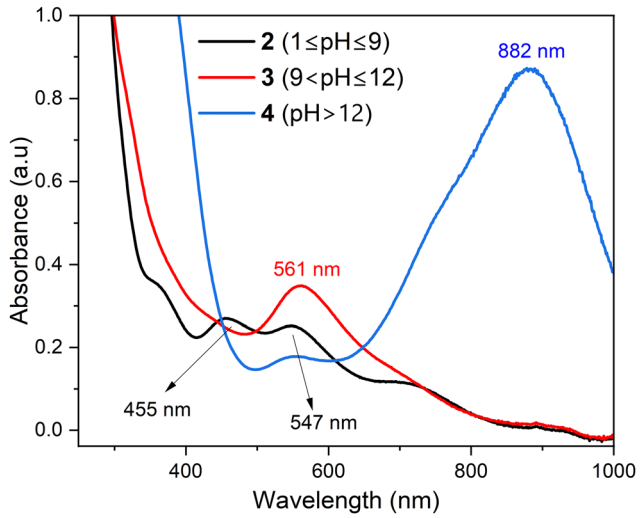

Fig. 4 Electronic spectra of 0.100 mM aqueous solutions compound $[Ru_3O(CH_3COO)_6(py)_2NO]PF_6$ (**2**) at various pH values after 30 minutes.

nucleophilic attack, indicate the low NO^+ character of the NO ligand in cluster **2**, experimentally corroborating the predominance of the Ru^{III}–NO^0 configuration proposed from molecular modelling results.[22]

An attempt was made to evaluate these successive equilibria under more controlled conditions using buffered solutions. However, in the presence of phosphate (PBS) and the tris (hydroxymethyl)-aminomethane molecule (TRIS.HCl buffer), the behaviour described above was not reproducible. One of the first hypotheses raised was the reaction of the species present in the solution at the different pHs with the salts that make up the buffer solutions. According to the literature, various species such as NH_2R, NH_2OH, N_2H_4, OH^-, HS^-, alcohols, phenols and thiolates can trigger nucleophilic attack reactions on NO and NO_2H sites.[42–45] Thus, based on the electronic spectra and p*K* values, a speciation curve was generated for species **2**, **3** and **4** (Fig. 6),[46] and a series of experiments were carried out to help elucidate the reactivity of nitrosyl **2** and verify the role of the nature of the reaction medium, pH

(1) $[\{RuNO\}^6Ru^{III}Ru^{III}O(CH_3COO)_6(py)_2]^+ + OH^- \rightarrow [Ru^{III}Ru^{III}Ru^{II}O(CH_3COO)_6(py)_2(HNO_2)]^0$ (Compound **3**: λ_{max} = 561 nm)

(2) $[Ru^{III}Ru^{III}Ru^{II}O(CH_3COO)_6(py)_2(HNO_2)]^0 + OH^- \rightarrow [Ru^{III}Ru^{III}Ru^{II}O(CH_3COO)_6(py)_2(NO_2)]^-$ (Compound **4**: λ_{max} = 882 nm)

Scheme 1

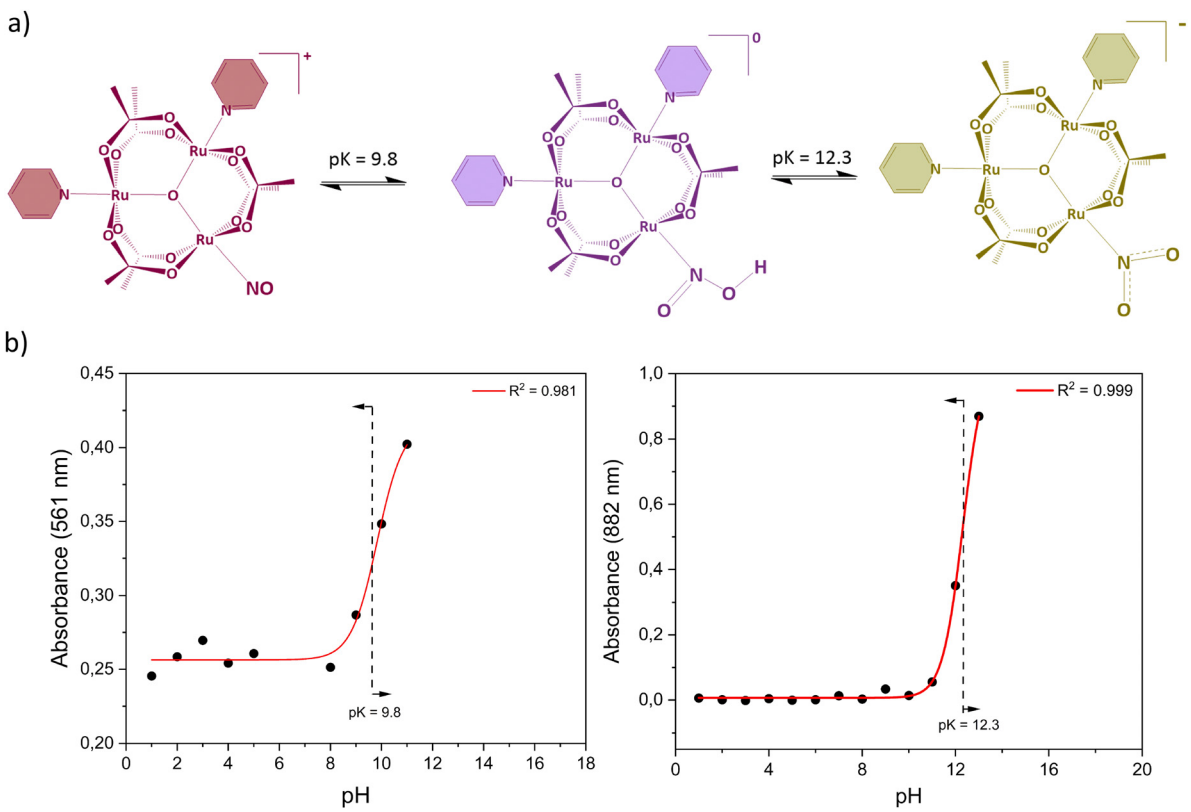

Fig. 5 (A) Proposed representative scheme for the nucleophilic attack reaction of the compound $[\{RuNO\}^6Ru^{III}Ru^{III}O(CH_3COO)_6(py)_2]^+$ by hydroxyl ions in aqueous media. (B) Sigmoidal fit of the spectrophotometric monitoring data collected for complex **2** (λ_{max} = 561 and 882 nm) in aqueous solutions at different values of pH.

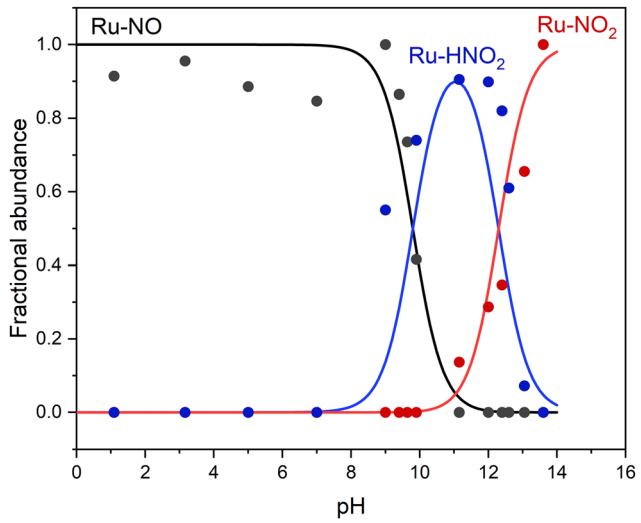

Fig. 6 Speciation curves of compounds **2**, **3** and **4** as a function of pH.

and the presence of other potential nucleophilic agents in addition to OH^- ions. Table 1 summarizes the conditions of the experiments carried out.

As seen in the first set of experiments in Table 1, in the absence of other reactants in solution, complex **2** responds to variations in the concentration of hydroxyl ions, predominating in solution at pHs below 9. Compound **3**, $[Ru^{III}Ru^{III}Ru^{II}O(CH_3COO)_6(py)_2(HNO_2)]^0$, begins to be observed in solution with pH ≥ 10, consistent with the speciation diagram (Fig. 6). In other words, OH^- ions are responsible for the nucleophilic attack on **2** under these conditions.

In the presence of phosphate and TRIS, at relatively short time intervals (30 minutes), compound **2** is observed in solution at pH 7.4. However, the system evolves towards observing a spectrum with absorption in the 560 nm region, characteristic of compound **3**, at a pH value where species **2** should largely predominate. The induction time and the dependence on the nature of the components in the reaction medium (exclusively OH^- ions or buffered solutions) to observe the product with absorption in the 560 nm region suggests a change in the way **3** is formed.

The need for **3** to be in solution in minimal quantities for the reaction to reach completion is confirmed when the experiment is carried out at pH 8.5 in TRIS.HCl buffer. In this condition, where the concentration of hydroxyl ions is higher, the induction time is shorter, and the predominance of **3** is observed from 30 min onwards (Table 1 and Fig. S9 and S10†). As a final control, the way of assessing the reactivity was changed. In the third set of experiments in Table 1, nitrosyl **2** was dissolved in solutions at pH 5 and 10, and their electronic spectra were recorded after 30 minutes. As expected, only **2** was observed at pH 5 and a mixture of **2** and **3** at pH 10. After this interval, a significant excess of tris(hydroxymethyl)-aminomethane (500 times) was added. At pH 5, where the initial concentration of **3** is virtually 0 (Fig. 6), no further formation of **3** is observed, even though the system is monitored for a long time (1 day). However, at pH 10, where there is a predominance of **3** (61%) over **2** (38.5%), the addition of a significant excess of both tris(hydroxymethyl)-aminomethane and Na_2HPO_4 immediately promotes total conversion to **3**.

The same analysis can be done in reverse by monitoring the reactivity of compound **4**, $[Ru^{III}Ru^{III}Ru^{II}O(CH_3COO)_6(py)_2(NO_2^-)]^-$, in aqueous solution. It was produced *in situ* by stoichiometric reduction of **1** with hydrazine. The reduced species $[Ru^{III}Ru^{III}Ru^{II}O(CH_3COO)_6(py)_2(NO_2^-)]^-$ does not persist, preventing the observation of its spectrum, suggesting a high reactivity of compound **4** in aqueous medium (Fig. 7). Upon the reduction reaction in buffered solu-

Table 1 Experimental conditions used to investigate the reactivity of compound **2**, $[\{RuNO\}^6Ru^{III}Ru^{III}O(CH_3COO)_6(py)_2]^+$. [**2**] = 0.100 mM; T = 298 K

pH	Solvent	Reactant	Time	Result
5.0[a]	H_2O	HCl/NaOH	30 minutes	Compound **2** persists in solution
7.0[a]	H_2O	HCl/NaOH	30 minutes	Compound **2** persists in solution
8.0[a]	H_2O	HCl/NaOH	30 minutes	Compound **2** persists in solution
9.0[a]	H_2O	HCl/NaOH	30 minutes	Compound **2** persists in solution
10[a]	H_2O	HCl/NaOH	30 minutes	Mixtures of compounds **2** and **3**
7.4	H_2O	Phosphate buffer[b]	30 minutes	Compound **2** predominates in solution
7.4	H_2O	Phosphate buffer[b]	125 minutes	Product with λ_{max} = 562 nm
7.4	H_2O	TRIS.HCl buffer[c]	30 minutes	Compound **2** predominates in solution
7.4	H_2O	TRIS.HCl buffer[c]	120 minutes	Product with λ_{max} = 563 nm
8.5	H_2O	TRIS.HCl buffer[c]	30 minutes	Product with λ_{max} = 565 nm
5.0[a]	H_2O	HCl/NaOH	30 minutes	Compound **2** persists in solution
5.0[d]	H_2O	TRIS(hydroxymethyl)-aminomethane[e]	Newly mixed	Compound **2** is stable in solution
5.0[d]	H_2O	TRIS(hydroxymethyl)-aminomethane[e]	1 day	Compound **2** is stable in solution
10[a]	H_2O	HCl/NaOH	30 minutes	Mixtures of compounds **2** and **3**
10[d]	H_2O	TRIS(hydroxymethyl)-aminomethane[e]	Newly mixed	Product with λ_{max} = 564 nm
10[d]	H_2O	Na_2HPO_4 [e]	Newly mixed	Product with λ_{max} = 567 nm

[a] pH adjusted with HCl or NaOH solutions. [b] PBS solution made from sigma-aldrich pellets (0.01 M phosphate buffer; 0.0027 M KCl; 0.137 M NaCl), yielding 100-fold excess of phosphate in relation to **2**. [c] Aqueous solution of tris(hydroxymethyl)-aminomethane 0.01 M (pH adjusted with small additions of HCl 1 M), yielding 100-fold excess of tris(hydroxymethyl)-aminomethane in relation to **2**. [d] Addition of tris(hydroxymethyl)-aminomethane or Na_2HPO_4 after 30 minutes. [e] 500-fold excess in relation to the concentration of **2**.

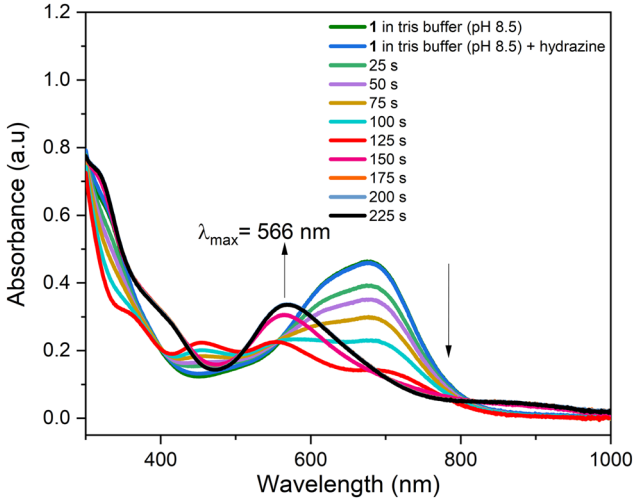

Fig. 7 Absorption spectra recorded during the reactivity experiment of complex **4** in TRIS.HCl buffer solution (50 mM, pH 8.5, T = 298 K).

tion (pH 8.5, TRIS.HCl buffer), what is observed is a decay of the band in the 700 nm region, characteristic of compound **1** ($[Ru^{III}Ru^{III}Ru^{III}O(CH_3COO)_6(py)_2(NO_2^-)]$, blue line), directly generating the spectral profile of nitrosyl **2** in 125 seconds ($[\{RuNO\}^6Ru^{III}Ru^{III}O(CH_3COO)_6(py)_2]^+$, red line). At this pH there is about 10% of **3** in solution. Thus, after 225 seconds, the spectral profile attributed to the total conversion from **2** to **3** emerges, with maximum absorption at 566 nm (black line).

The kinetics of the nucleophilic attack of **2** in different conditions gave us insight into a possible pathway. The results are shown in Fig. 8. In an aqueous medium, in the absence of other reactants and at pH 10, following the variation in absorbance of the signal with the highest intensity in the visible region (Fig. 8A), it can be seen that the spectra stop changing quite fast (about 5 minutes) and converge to a profile compatible with a mixture of **2** and **3**, comparable to the qualitative tests presented in Table 1. The plot of A *vs.* time shows a simple exponential profile. This behaviour is entirely expected and consistent with the speciation curve in Fig. 6. At this pH, very close to the pK for the conversion equilibrium of **2** to **3** (pK 9.8), there is a mixture of these two species, whose presence and relative amounts are determined by the pH, and the nucleophilic agent is undoubtedly the hydroxyl ions.

On the other hand, as shown in Fig. 8B and C, the kinetic plot for the reaction of **2** in lower pH and in the presence of the salts and reactants of the TRIS and phosphate buffers do not lead to conventional (pseudo)first-order kinetic curves. Since there is a superposition between the spectra of reactant and product, we plot the kinetic traces at 410 nm for the formation of product **3** and at 470 nm for the consumption of reactant **2**, to minimize the mutual interference (Fig. S11†). The first notorious thing is that, at pH 7.4, **2** should contribute largely (99.6%) to solution composition, while **3** is expected to be present in tiny amounts (0.4%). However, given enough time, the system evolves to form exclusively **3**.

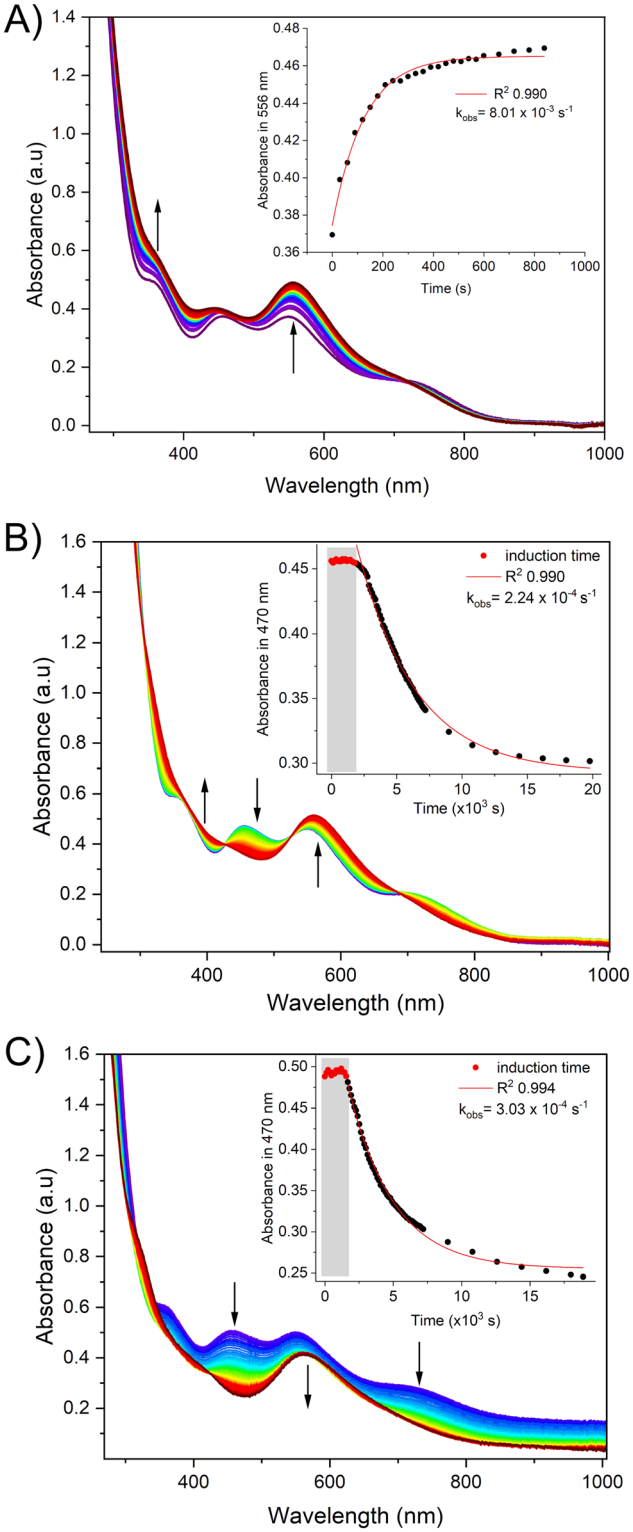

Fig. 8 (A) Absorption spectra during monitoring of the complex **2** in aqueous solution at pH 10 with the respective kinetic curve at 566 nm. (B) Absorption spectra during monitoring of complex **2** in TRIS.HCl buffer solution (0.01 M, pH 7.4) with the respective kinetic curve at 470 nm after 1680 s of induction time. (C) Absorption spectra during monitoring of complex **2** in PBS solution (0.01 M, pH 7.4) with the respective kinetic curve at 470 nm after 1560 s of induction time.

1. $[\{RuNO\}^6Ru^{III}Ru^{III}O(CH_3COO)_6(py)_2]^+ + OH^- \rightarrow [Ru^{III}Ru^{III}Ru^{II}O(CH_3COO)_6(py)_2(HNO_2)]$
2. $[Ru^{III}Ru^{III}Ru^{II}O(CH_3COO)_6(py)_2(HNO_2)] + \text{buffer} \rightarrow \mathbf{[Ru^{III}Ru^{III}Ru^{II}O(CH_3COO)_6(py)_2(HNO_2)].buffer}$
3. $[\{RuNO\}^6Ru^{III}Ru^{III}O(CH_3COO)_6(py)_2]^+ + [Ru^{III}Ru^{III}Ru^{II}O(CH_3COO)_6(py)_2(HNO_2)].\text{buffer} \rightarrow 2\,[Ru^{III}Ru^{III}Ru^{II}O(CH_3COO)_6(py)_2(HNO_2)]$

Scheme 2

Kinetic curves other than exponential ones can be associated with cooperative processes and provide information when analysing different types of chemical reactions.[47,48] In any case, the observed profile suggests at least two consecutive reaction steps in which the product of the first accelerates the formation of the second product. These products may be different, characterizing an autocatalytic example, or may be the same, characterizing a product acceleration reaction. In both cases, an induction period is observed, during which occurs the slow accumulation of catalytic quantities of a key intermediate. The symmetry between the reactant consumption and product formation curves strongly indicates it. Here, we do not observe the formation of **3** at pH 5, even with the addition of a significant excess of TRIS (Table 1).

The reactivity pattern shown above only begins at approximately pH 7.4, at which **3** is already present in the solution, albeit in tiny amounts. As said above, the symmetry between the consumption and formation curves (Fig. S11†) strongly indicates that, after the induction period (accumulation of the species that accelerate the formation of the final product), the formation of product **3** occurs at the expense of **2**. Other intriguing features might be highlighted. The final electronic spectra in TRIS and in PBS are the same, suggesting that the products of the reaction in both media are the same. Besides that, the induction times (as well as the k_{obs}, Fig. 8B and C) are almost the same, but it responds to OH^- concentration, being much smaller in pH 8.5 (Fig. S12†). Taken together, we ruled out the possibility that reactants other than the hydroxyl ions could be the nucleophilic agent. Instead, we suggest a model of two sequential steps (Scheme 2). Stage 1 is not a reactional step but a condition for further conversion of **2** to **3** in pHs below the pK value. Step (2) corresponds to the induction period preceding the reaction. We hypothesise that the buffer acts in step (2).

Recently, da Silva and co-workers demonstrated, through a theoretical–experimental approach, how the buffer composition affects the rates of nucleophilic attack in mononuclear ruthenium nitrosyls due to specific interactions of the buffer molecules (phosphate, imidazole and biphthalate) with the coordinated NO.[18] Nevertheless, they observe a conventional exponential kinetic trace in all cases, and the nucleophilic attack is performed at sufficiently high pH values for their case. Here, the site of interaction cannot be the nitrosyl **2**. Instead, we suggest that, in any experimental condition where **3** is present in the solution, it forms an intermediate species with the buffer, accelerating its formation from **2**. Further experiments are underway to unveil this proposal.

Conclusion

In this work, the reactivity of the trinuclear ruthenium complexes $[Ru_3O(CH_3COO)_6(py)_2NO_2]$ (**1**) and $[Ru_3O(CH_3COO)_6(py)_2NO]PF_6$ (**2**) in the aqueous environment were studied evaluating the chemical behaviour of these compounds under light irradiation and pH influence. The photochemical NO release was detected through chronoamperometry. Complex **1** showed a less substantial NO release compare to complex **2** which is due to the minor concentration of nitrite-O isomer compare to nitrite-N isomer. In addition to the NO release studies, we reported for the first time the interconversion of Ru–NO^+ to Ru–NO_2^- in trinuclear ruthenium acetates. By photometrically monitoring the complexes in solutions of different pHs, it was possible to obtain pK values for the interconversion. The nitrite complex **1** also displayed NO^+ release in the dark under acid conditions, readily producing the solvate-specie $[Ru_3O(CH_3COO)_6(py)_2S]^+$. Complex **2**, in deionized water, undergoes two successive nucleophilic attacks by hydroxyde ions, suggesting the formation of the $[Ru_3O(CH_3COO)_6(py)_2HNO_2]$ (**3**) and $[Ru_3O(CH_3COO)_6(py)_2NO_2]^-$ (**4**) species. However, compound **3** is formed in TRIS.HCl and phosphate buffered solutions at lower pH (pH 7.4 and 8.5) than the pK = 9.8 obtained for this species. This behaviour was tentatively assigned to the presence of buffers' salts, which influences the formation of compound **3**, leading to faster reaction rates after an induction period. Further experiments are underway to describe the unexpected behaviour of compound **2** towards its nucleophilic attack reaction.

Author contributions

H. E. Barbosa, A. B. da Silva and P. H. O. Nazar: conceptualization: formal analysis, investigation, methodology, writing – original draft, writing – review and editing. R. R. Bertoloni and A. G. S. de Oliveira-Filho: formal analysis, investigation, methodology; S. Nikolaou: conceptualization, data curation, formal analysis, investigation, methodology, writing – original draft, writing – review and editing, funding acquisition, project administration, supervision, validation, visualization.

Data availability

The data supporting this article have been included as part of the ESI.†

Conflicts of interest

The authors declare that they have no known competing financial interests or personal relationships that could have appeared to influence the work reported in this paper.

Acknowledgements

This paper was supported by the Brazilian agencies FAPESP – Fundação de Amparo à Pesquisa do Estado de São Paulo (2024/04574-6; 2020/15607-1, 2022/03478-8, 2023/10722-5, 2021/00675-4), CNPq – Conselho Nacional de Desenvolvimento Científico e Tecnológico (305761/2021-8, 309572/2021-5 and 131628/2021-6) and Capes – Fundação Coordenação de Aperfeiçoamento de Pessoal de Nível Superior (001) and Prof. Dr Roberto S. da Silva for the use os some equipment.

References

1 Y. Yu, S. Liu, L. Yang, P. Song, Z. Liu, X. Liu, X. Yan and Q. Dong, *MedComm*, 2024, **5**, e519.
2 H. Sies, V. V. Belousov, N. S. Chandel, M. J. Davies, D. P. Jones, G. E. Mann, M. P. Murphy, M. Yamamoto and C. Winterbourn, *Nat. Rev. Mol. Cell Biol.*, 2022, **23**, 499–515.
3 A. Tauffenberger and P. J. Magistretti, *Neurochem. Res.*, 2021, **46**, 77–87.
4 L. L. Camargo, F. J. Rios, A. C. Montezano and R. M. Touyz, *Nat. Rev. Cardiol.*, 2024, **22**, 20–37.
5 S. A. Sinenko, T. Y. Starkova, A. A. Kuzmin and A. N. Tomilin, *Front. Cell Dev. Biol.*, 2021, **9**, 714370.
6 Y. Hong, A. Boiti, D. Vallone and N. S. Foulkes, *Antioxidants*, 2024, **13**, 312.
7 B. Zhang, C. Pan, C. Feng, C. Yan, Y. Yu, Z. Chen, C. Guo and X. Wang, *Redox Rep.*, 2022, **27**, 45–72.
8 S. M. Andrabi, N. S. Sharma, A. Karan, S. M. S. Shahriar, B. Cordon, B. Ma and J. Xie, *Adv. Sci.*, 2023, **10**, 2303259.
9 G. R. Navale, S. Singh and K. Ghosh, *Coord. Chem. Rev.*, 2023, **481**, 215052.
10 L. K. Wareham, H. M. Southam and R. K. Poole, *Biochem. Soc. Trans.*, 2018, **46**, 1107–1118.
11 H. Alimoradi, K. Greish, A. Barzegar-Fallah, L. Alshaibani and V. Pittalà, *Int. J. Nanomed.*, 2018, **13**, 7771–7787.
12 J. Cheng, K. He, Z. Shen, G. Zhang, Y. Yu and J. Hu, *Front. Chem.*, 2019, **7**, 530.
13 C. F. N. da Silva, B. Possato, L. P. Franco, L. C. B. Ramos and S. Nikolaou, *J. Inorg. Biochem.*, 2018, **186**, 197–205.
14 R. Weinstain, T. Slanina, D. Kand and P. Klán, *Chem. Rev.*, 2020, **120**, 13135–13272.
15 S. Sun, J. Choe and J. Cho, *Chem. Sci.*, 2024, **15**, 20155–20170.
16 Z. A. Carneiro, J. C. Biazzotto, A. D. P. Alexiou and S. Nikolaou, *J. Inorg. Biochem.*, 2014, **134**, 36–38.
17 J. B. Godwin and T. J. Meyer, *Inorg. Chem.*, 1971, **10**, 2150–2153.
18 R. Rebecchi Rios, P. Gracielli Sousa Rodrigues, J. C. Biazzotto, S. E. Galembeck and R. Santana da Silva, *Eur. J. Inorg. Chem.*, 2022, **30**, e202200303.
19 F. S. Gouveia Júnior, A. S. de Sousa, R. B. da Silva, D. G. Rocha, E. H. Teixeira, M. Odorico de Moraes Filho, F. V. F. Jamacaru, H. Serra Azul Monteiro, R. J. B. Jorge, D. A. Wink, E. H. S. de Sousa and L. G. Luiz, *Eur. J. Inorg. Chem.*, 2024, **27**, e202300758.
20 N. C. Bessas, E . Christine de Souza Arantes, N. M. Cassani, U. E. Aquino Ruiz, I. A. Santos, D. O. Silva Martins, A. L. Costa Oliveira, G. A. Antoniucci, A. H. C. de Oliveira, G. De Freitas-Silva, A. C. Gomes Jardim and R. Galvão de Lima, *Nitric Oxide*, 2024, **147**, 26–41.
21 N. A. P. dos Santos, A. B. Silva, C. F. N. da Silva, A. D. P. Alexiou and S. Nikolaou, *New J. Chem.*, 2022, **46**, 4819–4826.
22 A. P. de Lima Batista, J. R. Pavan, M. A. Ribeiro and S. Nikolaou, *J. Mol. Struct.*, 2024, **1308**, 138119.
23 J. A. Baumann, D. J. Salmon, S. T. Wilson, T. J. Meyer and W. E. Hatfield, *Inorg. Chem.*, 1978, **17**, 3342–3350.
24 H. E. Toma, A. D. P. Alexiou and S. Dovidauskas, *Eur. J. Inorg. Chem.*, 2002, 3010–3017.
25 H. Ohtsu, N. Oka and T. Yamaguchi, *Inorg. Chim. Acta*, 2012, **383**, 1–6.
26 F. Neese, *Wiley Interdiscip. Rev.: Comput. Mol. Sci.*, 2018, **8**, e1327.
27 A. D. Becke, *J. Chem. Phys.*, 1997, **107**, 8554–8560.
28 F. Weigend and R. Ahlrichs, *Phys. Chem. Chem. Phys.*, 2005, **7**, 3297–3305.
29 V. Barone and M. Cossi, *J. Phys. Chem.*, 1998, **102**, 1995–2001.
30 S. Nikolaou, L. G. A. do Nascimento and A. D. P. Alexiou, *Coord. Chem. Rev.*, 2023, **494**, 215341.
31 N. Cacita, B. Possato, C. F. N. Da Silva, M. Paulo, A. L. B. Formiga, L. M. Bendhack and S. Nikolaou, *Inorg. Chim. Acta*, 2015, **429**, 114–121.
32 L. C. Ramos, J. C. Biazzotto and J. A. Uzuelli, in *Ruthenium Complexes as NO Donors: Perspectives and Photobiological Applications*, ed. A. Holder, L. Lilge, W. R. Browne, M. A. W. Lawrence and J. L. Bullock, Wiley-VCH Verlag GmbH & Co. KGaA, 2018, pp. 257–270.
33 M. C. L. Cândido, A. M. Oliveira, F. O. N. Silva, A. K. M. Holanda, W. G. Pereira, E. H. S. Sousa, Z. A. Carneiro, R. S. Silva and L. G. F. Lopes, *J. Braz. Chem. Soc.*, 2015, **26**, 1824–1830.
34 R. G. De Lima, M. G. Sauaia, D. Bonaventura, A. C. Tedesco, R. F. Vianna Lopez, L. M. Bendhack and R. S. Da Silva, *Inorg. Chim. Acta*, 2005, **358**, 2643–2650.
35 D. C. A. S. de Santana, T. T. Pupo, M. G. Sauaia, R. S. da Silva and R. F. V. Lopez, *Int. J. Pharm.*, 2010, **391**, 21–28.
36 A. M. Silva, L. B. Negri, J. C. Biazzotto, S. de Paula Machado, J. D. Santos, J. F. N. Batista, P. I. S. Maia, V. M. Deflon, L. M. Bendhack, M. R. Hamblin and R. S. da Silva, *J. Inorg. Biochem.*, 2023, **243**, 112166.
37 E. C. Fornari, M. S. P. Marchesi, A. E. H. Machado and S. Nikolaou, *Polyhedron*, 2009, **28**, 1121–1126.

38 W. Kaim, A. Das, J. Fiedler, S. Záliš and B. Sarkar, *Coord. Chem. Rev.*, 2020, **404**, 213114.
39 N. Lehnert, E. Kim, H. T. Dong, J. B. Harland, A. P. Hunt, E. C. Manickas, K. M. Oakley, J. Pham, G. C. Reed and V. S. Alfaro, *Chem. Rev.*, 2021, **121**, 14682–14905.
40 M. J. Moorcroft, J. Davis and R. G. Compton, *Talanta*, 2001, **55**, 785–803.
41 J. Sun, X. Zhang, M. Broderick and H. Fein, *Sensors*, 2003, **3**, 276–284.
42 L. Dizsa, V. Kormos and M. T. Beck, *Inorg. Chim. Acta*, 1984, **82**, 69–74.
43 M. M. Gutiérrez, J. A. Olabe and V. T. Amorebieta, *Eur. J. Inorg. Chem.*, 2012, **48**, 4433–4438.
44 M. M. Gutiérrez, V. T. Amorebieta, G. L. Estiú and J. A. Olabe, *J. Am. Chem. Soc.*, 2002, **124**, 10307–10319.
45 S. A. Suarez, N. I. Neuman, M. Muñoz, L. Álvarez, D. E. Bikiel, C. D. Brondino, I. Ivanović-Burmazović, J. L. Miljkovic, M. R. Filipovic, M. A. Martí and F. Doctorovich, *J. Am. Chem. Soc.*, 2015, **137**, 4720–4727.
46 H. Y. Samayoa-Oviedo, S. A. Mehnert, M. F. Espenship, M. R. Weigand and J. Laskin, *J. Chem. Educ.*, 2023, **100**, 815–821.
47 L. Bentea, M. A. Watzky and R. G. Finke, *J. Phys. Chem. C*, 2017, **121**, 5302–5312.
48 M. P. Mower and D. G. Blackmond, *J. Am. Chem. Soc.*, 2015, **137**, 2386–2391.